Messages From the Small Intestine Carried by Extracellular Vesicles in Prediabetes: a Proteomic Portrait

Author(s) Names

Inês Ferreira[1,2,3#], Rita Machado de Oliveira[1#], Ana Sofia Carvalho[1], Hans Christian Beck[4], Rune Matthiesen[1], Bruno Costa-Silva[3,*,#], Maria Paula Macedo[1,5,6,*,#]

Author(s) Address Information

1. *Chronic Diseases Research Centre, CEDOC, NOVA Medical School, (NMS/FCM), Lisbon 1169-056, Portugal*
2. *Bioengineering – Cell Therapies and Regenerative Medicine PhD Program, Instituto Superior Técnico, University of Lisbon, Lisbon 1049-001, Portugal*
3. *Champalimaud Research, Champalimaud Centre for the Unknown, 1400-038 Lisbon, Portugal*
4. *Centre for Clinical Proteomics, Department of Clinical Biochemistry and Pharmacology, Odense University Hospital, Denmark*
5. *APDP-ERC Portuguese Diabetes Association Education and Research Centre, Lisbon 1250-189, Portugal*
6. *Departament of Medical Sciences, University of Aveiro, Aveiro 3810-193, Portugal*

Symbol

[#] Equal contribution

[*] Corresponding author(s)

E-mail: bruno.costa-silva@research.fchampalimaud.org (Costa-Silva B), paula.macedo@nms.unl.pt (Macedo MP).

Abstract

Extracellular vesicles (EVs) mediate cell-cell communication in a variety of physiological and pathological conditions. In the pathogenesis of type 2 diabetes, inter-organ communication plays an important role in its progress and metabolic surgery leads to its remission. Gut dysbiosis is emerging as a diabetogenic factor. However, it remains unclear how gut senses metabolic alterations and whether this is transmitted to other tissues via EVs content. In this study, using a diet induced-prediabetic mouse model, we observed that protein packaging in gut derived extracellular vesicles (GDE), specifically at the small intestine, is increased in prediabetes compared to GDE from healthy mice. Moreover, there were significant differences in GDE proteins between the two conditions. Proteins related to lipid metabolism and to oxidative stress management were more abundant in prediabetic GDE compared to those of healthy mice. On the other hand, proteins related to glycolytic activity, as well as those responsible for the degradation of polyubiquitinated composites in the proteasome, were depleted in prediabetic GDE compared to those of healthy mice. Together, our findings show that protein packaging in GDE is markedly modified during prediabetes pathogenesis. Thus, suggesting that prediabetes alterations in small intestine are translated into GDE with a modified protein cargo which are dispersed into the circulation where they can interact with and influence the metabolic status of other tissues. This study highlights the importance of the small intestine as a tissue that can propagate the metabolic dysfunctions of prediabetes throughout the body and the importance of GDE as the messenger.

KEYWORDS: Small Instestines; Exosome; Type 2 diabetes; Lipids; Diet

76 # Introduction

77 Type 2 diabetes (T2D) is the most common chronic metabolic disease characterized by high blood
78 glucose and it accounts for 95% of diabetes cases in adulthood [1]. The escalating incidence of
79 T2D as a consequence of sedentary lifestyle and over-nutrition, imposes a substantial burden to
80 health care systems worldwide. Among the therapeutic interventions, metabolic surgery which
81 targets the small intestine, is the most effective procedure in diabetes remission [2;3]. Prediabetes
82 is a high-risk state for T2D, and it is defined by glycemic levels higher than normal, but lower
83 than diabetic limits [4]. This stage can be seen as a fork in the road, if left untreated, the likelihood
84 for progression to diabetes is high. Importantly, with timely diagnosis and with patient's
85 compliance to lifestyle intervention, prediabetes can be reversed [5]. Obesity is a potent risk factor
86 for diabetes. Moreover, a diet rich in fat and sugar, with large intake of finely processed grains
87 and starchy carbohydrates is directly associated with this disease [6].

88 Blood glucose homeostasis requires a constant communication between insulin-secreting and
89 insulin-sensitive organs. Failure in the coordination between these organs can lead to a rise in
90 blood glucose levels and to prediabetes. Recently, extracellular vesicles (EVs) emerged as an
91 important component of organismal communication and have been implicated in the
92 pathophysiology of diabetes [7]. These small vesicles are able to transfer proteins and nucleic
93 acids from a releasing cell to a distant target cell, thus modulating gene and protein expression
94 and leading to functional changes [8-9]. Interestingly, visceral adipose tissue derived EVs trigger
95 systemic inflammation, glucose intolerance and insulin resistance; hallmarks of prediabetes [10].
96 In obese patients, adipose tissue-EVs were able to modulate insulin responses in hepatocytes and
97 muscle cells [11].

98 The intestinal system is daily exposed to food, millions of pathogens, and high concentrations
99 of foreign antigens. In the case of the gut EVs, the composition and effects of EVs released by
100 the resident microbiota have been explored [12-13]. For instance, these EVs are released into the
101 gut mucosa and participate in local innate responses to invading bacteria through microbicidal
102 activity [14] and mediate gut permeability through the regulation of tight junctions [15]. While
103 the contribution of microbiota is crucial to maintain intestinal homeostasis, the epithelial cells are
104 a critical component of the intestinal defense system forming a selective permeable barrier,
105 allowing the absorption of nutrients, electrolytes and water, and blocking ingress of toxins and
106 antigens. Epithelial cells in the gut were described to secrete EVs and up today they were
107 described to play a role as antigen-carrying structures [16]. Whether EVs derived from the small
108 intestine play a primordial role as a diabetogenic trigger needs to be elucidated. In fact, the
109 relevance of the gastrointestinal tract in diabetes is elucidated by the fact that metabolic surgery
110 improves glucose homeostasis more effectively than any known pharmaceutical or behavioral
111 approach, causing durable remission in many patients with T2D [17]. Attempts to elucidate the

exact mechanism by which gastro-intestinal surgery reverses T2D have implicated changes in the gut hormones, bile acid metabolism, intestinal nutrient sensing and metabolism, gut microbiota, and other factors [18]. Gut dysbiosis recently emerged as a possible player in the development of T2D [19]. Despite the literature on the impact of microbiota in T2D onset and development, the role of the small intestine EVs, independent of EVs derived from the biota is still elusive. While gut derived EVs (GDE) are considered to play an important role in intestinal diseases [20] it is not known how GDE protein content is modulated by a western diet. Therefore, it is timely to understand the importance of the small intestine as a metabolically active organ in prediabetes and the means by which it communicates with other tissues via EVs. Here we aim at characterizing the differences in the GDE proteome of diet-induced prediabetic mice compared to that of healthy mice fed standard chow.

Results

Description of the prediabetes mouse model

First, we established a mouse model that recapitulates many features of prediabetes [21]. High fat and sugar feeding leads to obesity, hyperinsulinemia and glucose intolerance. Therefore, we used an hypercaloric diet (HD) which composition is 58% fat and 18 % sucrose, in contrast with normal-chow diet (NCD) that is 11% fat with no added sugar. After 12 weeks of diet, HD mice demonstrate significantly increased body weight (Figure 1A, 1B) and an abnormal intrahepatic fat accumulation – a hallmark of liver steatosis (Figure 1C). They also developed glucose intolerance, evaluated by a glucose tolerance test in the previous week of sacrifice and correspondent area under the curve for each group (Figure 1D, 1E) (**Figure 1**).

Characterization of intestine derived extracellular vesicles

Once the prediabetic phenotype was validated in the diet-induced obese animals, we evaluated the presence of EVs in small intestine. We stained cross sections for CD81, a commonly used EV-marker, and the presence of this protein was detected in similar levels in the lumen of the intestine in both conditions (NCD and HD fed mice - Figure 1F). Moreover, western blot was performed to confirm the enrichment of CD63, a commonly used EV marker, in GDE from NCD and HD when compared with the tissue (Figure 1G). Next, GDE were characterized by nanoparticle tracking analysis and total amount of protein was quantified by BCA. The mean size of the particles, in both conditions, was around 100 nm (NCD=152.8±67.5; HD=128.6±50.7) (Figure 1H). While the number of EVs is decreased in HD animals (Figure 1I), protein cargo was higher in GDE isolated from HD-fed mice (HD-GDE) than in NCD-fed (NCD-GDE) mice (Figure 1J). Interestingly, the amount of protein per GDE was higher in prediabetic mice than in controls (Figure 1K) (**Figure 1**).

149
150 **Proteomics Study**

151 EVs protein cargo provides valuable information regarding the cellular environment where they
152 are produced [22]. We proposed that a diet induced dysmetabolic environment modulates the
153 protein composition of GDE. Thus, to identify the impact of the diet-induced prediabetic gut
154 milieu on GDE protein cargo, we isolated GDE (Supplementary Figure1) from mice under HD
155 and respective controls and analysed it by mass-spectrometry (MS) (Supplementary Figure 2A).
156 Potential contribution of gut bacteria EVs was ruled out by mass spectrometry analysis, which
157 showed absence of bacterial proteins (Supplementary Figure 2B), and culture of gut conditioned
158 media in antibiotics-free agar, which did not display bacterial growth (Supplementary Figure 2C).
159
160 **Bioinformatics analysis of the MS identified proteins**

161 After filtering the identified proteins for reverse proteins used for false discovery rate and possible
162 contaminating proteins (e.g. keratin and bovine proteins from cell culture media), we identified a
163 total of 2467 proteins after removing isoforms from the same gene. Intensity based absolute
164 quantitation (iBAQ) was calculated [23]. Excluding proteins with missing quantification values
165 resulted in 2156 proteins (Supplementary file). The raw data was then normalized (Figure 2A).
166 Subsequently, we distinguished between identified and regulated proteins. Regulated proteins are
167 those at least two-fold regulated and with an adj. p-value < 0.05. After applying the
168 aforementioned criteria to our data set, we obtained a list of robustly regulated 558 proteins, which
169 shows that diet-induced prediabetes alters the protein composition of GDEs (Figure 2A). All data,
170 before applying the filtering criteria, is represented in a volcano plot that describes the level of
171 significance and magnitude of changes observed, comparing the HD with the NCD group (Figure
172 2B). The dotted line in the plot represents the threshold of adj.p-value<0.05, and from that line
173 above each individual dot represents a protein within the 558 regulated ones.
174
175 **Gene Ontology**

176 To gain insight into the biological role of the 588 regulated proteins, we performed Gene
177 Ontology and Kyoto Encyclopedia for Genes and Genomes (KEGG) enrichment analysis, which
178 revealed that the vast majority of proteins were related with metabolism. In terms of molecular
179 function, enzyme activity (including isomerases, hydrolases and oxidoreductase) shows up in the
180 top of list (Figure 3A). Most of the enriched pathways for gene ontology biological process
181 emphasized lipid metabolism, highlighting fatty acids (FA) β-oxidation. Curiously, glycolysis-
182 related and proteolysis in cellular protein catabolic processes-related proteins are mostly down
183 regulated (Figure 3B). Considering KEGG pathways enrichment analysis, the affected proteins
184 belong primarily to FA, carbohydrate and amino acid metabolism. Interestingly, alcoholism-
185 related proteins show up with great significance (Figure 3C). In terms of down regulated proteins,
186 based on the KEGG analysis the proteasome and focal adhesions proteins are markedly down

regulated. Finally, to assess sub-cellular localization of the GDE protein cargo regulated by diet we used gene ontology cellular component analysis and found that the majority of altered proteins are mitochondrial, followed by the cytosolic ones. Once again, proteasome related proteins were down regulated (Figure 3D).

Cluster analysis for GDE regulated proteins

For a more detailed characterization of GDE proteome, we looked into the subset of proteins that were overly altered among groups. For that, we established an adj.p-value<0.0001 as cut-off (Figure 4A). The proteins with that significance are represented in the heatmap (Figure 4B). To gain insight into protein-protein interaction of GDE identified protein cargo, we used the STRING software to link some of the altered proteins and to display the level of relationship between them. The proteins that demonstrate higher level of interaction are the ones related with the proteasome, including both α subunits (PSMA) and β (PSMB). Actin related proteins, which function is to maintain cellular integrity, also display relevant interaction. Moreover, network analysis highlights strong tendency towards metabolic-related proteins (Supplementary Figure 2). The fold change of all altered proteins varied up to 2-fold when comparing HD with NCD GDE. Within metabolic pathways, the altered proteins are mainly involved in nutrient metabolism, such as glucose, FAs and amino acids. In addition, cell integrity, focal adhesion and proteasome-related proteins are all down regulated (Figure 4C and Supplementary Figure 4). Key GDE proteins up and down regulated by HD are also represented in their subcellular location (**Figure 5**). Noteworthy to mention, proteins related with carbohydrate metabolism, which ensures the supply of energy to the cells (PFKL, ALDOA, ALDOB, PGAM2, ENO1, PGM5), with the tricarboxylic acid (TCA) cycle (DLST, IDH1). cholesterol homeostasis (ACAT1, ACAT2) and proteasome (PSMA1, PSMA2, PSMA3, PSMA4, PSMA5, PSMA6, PSMA7, PSMB1, PSMB2, PSMB3, PSMB8, PSMB10) are down regulated by HD. On the other hand, proteins related with lipid homeostasis (ACOT1 ACOT2, ACOT3, ACOT5, ACOT6), FA mitochondrial β-oxidation (HDHA, ACADVL, ACADL, ECHS1, ACAA2), very-long chain FA peroxisomal β-oxidation (ECH1, ACOX1), amino acids metabolism (GSTA1, GSTA2) and antioxidant defence (ALDH2, ALDH1B1, PRDX6, GSTA4, GSTM2) are majorly upregulated. **Table 1** describes all the proteins up and down regulated according to their biological function.

Discussion

The relationship between diet composition and the incidence of metabolic disorders is a public health concern. One of the first organs and by far the largest one to contact with food and its derivates is the gut, as a consequence it is where the first organismal response should be found [24]. Here, we report that GDE isolated from animals fed an HD, mimicking the western one,

224 have a distinct proteome that strongly reflects the intestinal dysmetabolic milieu. We found
225 numerous pathways associated with macronutrients altered in GDE isolated from HD-fed mice;
226 of great relevance the ones related with lipidic and carbohydrate metabolic processes.
227
228 From the enrichment analysis we observed that both glycolysis-gluconeogenesis and pyruvate
229 pathways are within the most affected ones (Figure 3B). Rate limiting enzymes for glycolysis
230 were found to be less abundant, namely hexokinase (HK) and phosphofructokinase (PFKL), thus
231 suggesting changes in glucose utilization and lactate production. In accordance, in diabetic rats,
232 phosphorylation of glucose is inhibited in tissues such as the heart, skeletal muscle and liver [25;
233 26; 27; 28]. Interestingly, in hearts from diabetic rats, PFK and HK down regulation is reverted
234 by an oral anti-diabetic drug - metformin [29]. We suggest that the observed decreased levels of
235 PFKL in prediabetic GDEs is reflecting a similar down regulation in the small intestine of
236 prediabetic mice and is an early event in the progression of the disease [30]. Down in the
237 glycolysis pathway, pyruvate dehydrogenase A1 (PDHA1), which belongs to the PDH complex,
238 was upregulated in HD GDEs, indicating a possible compensation in the pathway given the
239 importance of acetyl-CoA for the TCA cycle and for many other proteins and lipidic biochemical
240 reactions. PDH is fundamental for metabolic flexibility, the ability of switching from
241 carbohydrates to lipid fuel as energy sources, and the inability of cells to do so is an important
242 hallmark of T2D [31]. Our results suggest that in the early stages of the disease gut cells tackle
243 the insult of HD feeding by changing the source of fuel. The decrease in glycolysis might be
244 explained by the low amount of fibers provided by the diet; since the percentage of fibers in HD
245 is considerably reduced and in part replaced by sucrose. Likewise, fibers have a beneficial effect
246 on NCD mice, by improving intestinal integrity, enhancing energy expenditure and reducing
247 inflammation [32]. In fact, because HD has increased sucrose, we envisage that sucrose is being
248 directed to an alternative pathway, such as de novo lipogenesis, known to also occur in the gut
249 [33].
250
251 In accordance with the high lipidic content present in the HD, we observed that lipid metabolism
252 (biosynthesis of unsaturated FA and FA elongation) is vastly altered. The excess of fat in the diet
253 is known to cause increased fatty acids uptake, which can be either metabolized for the production
254 of energy or, when in excess, will be stored. Several proteins involved in mitochondrial β-
255 oxidation (HADHA, ACADVL, ACADL, ECH1, ECHS1), which generates acetyl-CoA to feed
256 the TCA cycle, and peroxisome β-oxidation (ECH1, ACOX1), major fatty acids degradative
257 pathway, are upregulated in GDE by HD, suggesting that fatty acids are favoured as energy source
258 over glucose (Figure 5). In addition, over-activation of lipid metabolism related pathways is a
259 common feature of obesity and T2D, leading to a state of hyperglycemia [34; 35; 36]. Moreover,
260 a family of acyl-CoA thioesterases (ACOTs) were particularly upregulated; these are
261 intermediaries in the decision whether fatty acids are directed to the TCA cycle or stored, (Figure

262 5, Supplementary Figure 4) [37; 38]. Altogether, this suggests that HD shifts the burden of energy
263 provision from carbohydrates toward fat derived from diet, since ACSS2 (a protein that conducts
264 fatty acids to the TCA cycle) is down regulated and PDHA1 (which provides a link between
265 glycolysis, TCA cycle and lipogenesis) is upregulated in order to ensure the energetic need of the
266 cell. Based on recent literature, obesity-induced activation of ACOTs directs fatty acids towards
267 triglycerides synthesis for incorporation into chylomicrons or VLDL particles [39; 40].
268 Noteworthy, some studies consider activation of ACOTs protective against fatty acids over-
269 supply, slowing the flux of fatty acids to downstream metabolic pathways [41; 42; 43]. Whether
270 this is the case in the gut, needs to be further explored. Additionally, intestinal cells in the HD
271 model appear to prioritize production of energy from fatty acids, instead of carbohydrates. This
272 is shown by the upregulation of ATP-citrate lyase (ACLY), an enzyme responsible for the
273 conversion of citrate to acetyl-CoA – the first step in DNL. Overall, the major enzymes found
274 altered within the gut EVs are very much responsible for regulating acetyl-CoA levels in the cells,
275 given that this molecule is a fundamental node in metabolism, in the future it would be of major
276 interest to quantify it in enterocytes.
277
278 Increased fatty acids oxidation promotes mitochondrial dysfunction, as well as fatty acids
279 peroxidation and glucose dysmetabolism, altogether leading to reactive oxygen species (ROS)
280 accumulation to pernicious levels [44]. Oxidative stress is implicated in various diseases
281 including diabetes [45]. We observed several proteins involved in antioxidant defense
282 mechanisms, such as removal of free radicals (PRDX6) and elimination of xenobiotic compounds
283 and products of lipids peroxidation (GSTA4, GSTM2) upregulated in HD-GDE, suggesting an
284 activation of an antioxidant response in the gut cells (Figure 5). Consistent with our model, the
285 presence of numerous isoforms of the aldehyde dehydrogenase (ALDH) family was upregulated
286 in HD-derived GDE. ALDHs are a family of oxidizing enzymes responsible for cellular
287 detoxification by oxidation of biogenic and xenogeneic aldehydes that accumulate through
288 metabolism [46]. In particular, we highlight ALDH1B1 due to its ability to metabolize
289 acetaldehyde and maintain glucose homeostasis [46]. Of interest, ALDH2 has been explored as a
290 pharmacological target, due to its role in cellular damage defense against oxidative stress induced
291 by pathological conditions, for instances high glucose [47].
292
293 Besides glucose and fatty acids, amino acids, in particular lysine, also play important roles in
294 providing energy to gut epithelial cells (Figure 3C) [48]. Lysine, which pathway we see affected
295 in HD-GDE, mediates protein biosynthesis, such as of carnitine, a key factor in fatty acid
296 metabolism [49]. Interestingly, carnitine deficiency due to poor lysine diet induces triglycerides
297 accumulation [50]. Evidence that the HD not only induces obesity, but also a general pathological
298 state arises from the massive alteration of proteasome-related proteins. The proteasome is
299 recognized as an important target in many diseases [51]. Our data showed down regulation of

proteasome proteins, which is consistent with decreased proteasome function reported in a broad array of chronic diseases (Figure 3C; 5) and defective degradation of damaged proteins, a hallmark of neurodegenerative diseases [52]. One hypothesis is that the decreased content of proteasome proteins in prediabetic GDE mirror in the cell of origin. Alternatively, the GDE producing cells can be consuming proteasome to counteract the deleterious effects of oxidative stress, resulting in lower packaging of proteasome proteins in GDEs.

The present study is the first comprehensive analysis of GDE protein content. We found that diet composition strongly modulates GDE proteomic profile. Several lines of evidence support a model in which the metabolic alterations induced by the HD are translated in a similar manner in alterations in GDE protein cargo. These results bring light into the important modification taking place in the small intestine and how it translates into GDE content. We propose that future studies should focus on whether GDE can act in local and distant cellular targets and mediate prediabetes. We also propose that the analysis of GDE in biofluids may represent a strategy to non-invasively detect metabolic modifications in the gut linked with prediabetes and potentially be employed early diagnose and follow-up prediabetes patients.

Material and methods

Animals

Male C57Bl/6J mice were housed in a temperature-controlled room, in a 12-hour light/dark cycle. For induction of prediabetic phenotype, C57BL/6J mice started on a high-fat diet at 6 weeks of age, with free access to food and water, for 12 weeks. Hypercaloric diet (HD) (OpenSource Diet, D12331) composition is 16.5% protein, 25.5% carbohydrate, and 58% fat with 13% addition of sucrose. The control normal chow diet (NCD) (Special Diets Services, RM3) composition is 26.51% proteins, 62.14% carbohydrates and 11.35% fat and no sucrose. At 18 weeks of age, 12 weeks of diet, mice were sacrificed. Mice were anesthetized using 2% isoflurane. Mice were sacrificed under 12 hours of fasting, with a previous feeding period of 2 hours, with the previous 8 hours of fasting. Blood, liver and small intestine were collected from prediabetic mice and respective controls. All animals were treated according with National and European Union Directive for Protection of Vertebrates.

Glucose Tolerance Test

At week 11 of diet GTT was performed. Mice were fasted overnight and weighed in the morning. Mice were then given an intra-peritoneal injection of a glucose solution (20% m/v – Sigma Aldrich) at 2g/kg body weight. Serum blood glucose levels were measured at 15, 30, 60, 90 and 120 min after injection. Blood glucose levels we measured using OneTouch Ultra glucose meter (LifeScan Inc).

Small Intestine Histology

After sacrifice, liver and small intestine were washed in PBS and fixed for histology and a portion of small intestine was snap frozen in liquid nitrogen for later analysis by western blot. The clean gut was placed in 2% Paraformaldehyde with 20% Sucrose, overnight at 4ºC; washed three times in Phosphate Buffered Saline (PBS), 10 min each; transferred to 30% sucrose for 2 hours at 4ºC; left overnight at 4ºC in Optimal Cutting Temperature compound (OCT) with 30% Sucrose (1:1). In the following day, tissues were embedded in 20% Sucrose (1:4) + (OCT) (3:4) in the presence of dry ice and immediately stored -80ºC. Consequently, tissues were sliced into 6 µm thin sections in the cryostat and stored at -80ºC for following applications. Gut samples were used for CD81 staining and liver samples for Hematoxylin-Eosin staining.

Exosomes Isolation and Nanoparticle Tracking Analysis

After sacrifice the small intestine was removed, washed with PBS and cultured overnight, at 37ºC and 5%CO2, in RPMI medium (Sigma) supplemented with 1% Penicillin/Streptomycin and 10% Fetal Bovine Serum EV-free, to avoid contaminations from serum EVs. In the following day

355 medium was collected. Conditioned medium was submitted to two initial centrifugations (10 min,
356 500 g and 20 min, 3 000 g) to remove any suspended or dead cells in the medium. To remove
357 large EVs, media was centrifuged (20 min, 12 000 g) and the pellet was discarded. The
358 supernatant enriched in small EVs was again centrifuged (2 h 20 min, 100 000 g), and the EVs
359 enriched pellet was collected. For sucrose cushion purification, this pellet was resuspended in 14
360 mL filtered phosphate buffered saline (PBS, Corning 15313581, NY, US) and added the top of 4
361 mL sucrose solution (D2O containing 1.2 g of protease-free sucrose and 96 mg of Tris base
362 adjusted to pH 7.4). A new ultracentrifugation was performed (1 h 10 min, 100 000 g), after which
363 4 mL of the sucrose fraction was collected using a 18 G needle placed at the bottom of the
364 ultracentrifugation tube (away from the pellet). Finally, 16 mL of PBS were added to the collected
365 sucrose/EVs solution and an overnight (16 h, 100 000 g) ultracentrifugation was performed. The
366 pellet containing the isolated EVs was resuspended in filtered PBS. The concentration and size
367 of EVs were analyzed in NanoSight NS300 (NS3000) system equipped with a blue laser (405
368 nm), according to the manufacturer's instructions. EVs were diluted 1:1000 in filtered sterile PBS.
369 Each sample analysis was conducted for 90 seconds and measured 5 times using Nanosight
370 automatic analysis settings. The software calculated the size distribution in nanometers and the
371 concentration in number of particles per mL.
372
373 **Western Blotting**
374 Protein extracts for western blot analysis were obtained using cold lysis buffer (20 mM Tris- HCl
375 pH 7.4, 5 mM EDTA pH 8.0, 1% Triton-X 100, 2 mM Na3VO4, 100 mM NaF, 10 mM Na4P2O7)
376 in the presence of protease inhibitors (completeTM, Mini, EDTA-free Protein inhibitor cocktail
377 tablets, Roche, Sigma). Gut tissue and GDE were homogenized in the lysis buffer and sonicated
378 three time for 30 seconds each at 10 µm amplitude, incubated on ice between each sonication
379 step. Lysates were centrifuged at 18.000 g for 10 min at 4°C. Soluble fraction was collected and
380 protein concentration was determined using the PierceTM BCA Protein Assay kit (Thermo
381 Fisher). For protein expression analysis, equal amounts of total protein (20 µg) were mixed with
382 sample buffer (250 mM Tris-HCl pH 6.8, 8% SDS, 40% glycerol, 8% β-mercaptoethanol,
383 bromophenol), before being denaturated at 95ºC for 10 min. Samples were then resolved by an
384 8% sodium dodecyl sulfate-polyacrylamide gel electrophoresis (SDS-PAGE). Proteins were
385 subsequently electrotransferred to a polyvinylidene fluoride (PVDF) membrane (Immobilon-P
386 Membrane, PVDF, Millipore) for 20 min at 25 mA and 2,5 mV in a Trans-Blot Turbo TM
387 Transfer System (BioRad). Membranes were blocked for 1 hour at RT with 3% BSA (Thermo
388 Fisher) in tris-buffered saline with 0,1% Tween (TBS-T) (blocking solution). Membranes were
389 incubated overnight at 4ºC, with CD63 antibody (Santa Cruz Biotechnology) prepared in 3% BSA
390 in TBS-T, diluted 1:1000. Membranes were washed three times with TBS-T and incubated for 1
391 hour at RT with the secondary antibody anti-rabbit antibody diluted 1:5000 (Santa Cruz

392 Biotechnology). Blots were developed with ECL (ECL Prime, GE Haelthcare) according to
393 manufacturer's instructions. Chemidoc Touch (Biorad) was used to detect chemilumunescence.
394 Band intensities were quantified usinf ImageLab software and normalized by β-actin as a loading
395 control.
396
397 **Nano-LC-MSMS analysis**
398 Peptide samples were analysed by nano-LC-MSMS (Dionex RSLCnano 3000) coupled to a Q-
399 Exactive Orbitrap mass spectrometer (Thermo Scientific). Briefly, 5 µL of sample was loaded
400 onto a custom made fused capillary pre-column (2 cm length, 360 µm OD, 75 µm ID) with a flow
401 of 5 µL per min for 7 min. Trapped peptides were separated on a custom made fused capillary
402 column (20 cm length, 360 µm outer diameter, 75 µm inner diameter) packed with ReproSil Pur
403 C18 3-µm resin (Dr. Maish, Ammerbuch- Entringen, Germany) with a flow of 300 nL per minute
404 using a linear gradient from 92 % A (0.1% formic acid) to 28 % B (0,1% formic acid in 100
405 acetonitrile) over 93 min followed by a linear gradient from 28 % B to 35 % B over 20 min at a
406 flowrate of 300 nl per minute. Mass spectra were acquired in positive ion mode applying
407 automatic data-dependent switch between one Orbitrap survey MS scan in the mass range of 400
408 to 1200 m/z followed by HCD fragmentation and Orbitrap detection of the 15 most intense ions
409 observed in the MS scan. AGC target value in the Orbitrap for MS and MSMS scans were
410 1,000,000 ions at a resolution of 70,000 at m/z 200 for MS scans, and 25,000 ions at m/z 200 for
411 MSMS scans. Peptide fragmentation in the HCD cell was performed at normalized collision
412 energy of 31 eV. Ion selection threshold was set to 5,000 ions for MSMS analysis, and maximum
413 injection time was 100 ms for MS scans and 200 ms for MSMS scans. Selected sequenced ions
414 were dynamically excluded for 60 seconds.
415
416 **MSMS analysis**
417 Mass accuracy was set to 5 ppm on the peptide level and 10 Da on the fragment ions. A maximum
418 of four missed cleavages was used. Carbamidomethyl was set as a fixed modification. M
419 oxidation, N-terminal protein Acetyl, Q Deamidation and N Deamidation were set as variable
420 modifications. The MSMS data was searched against all reviewed mouse proteins from UniProt
421 with concatenation of all the sequences in reverse maintaining only lysine and arginine in place.
422 The data was searched and quantified with both MaxQuant [53] and VEMS [54].
423
424 **Statistical Analysis**
425 Data are presented as means ± SEM. GTT curves, bar plots, volcano plots, heatmap and linear
426 regression analyses were done using GraphPad Prism 8 (GraphPad Software). Differences
427 significance was calculated through unpaired student's t tests with Welch's correction; one-way

ANOVA followed by Tukey-Kramer multiple comparison tests. Differences were accepted as statistically significant at $p<0.05$.

Author's contributions

IF and RMO carried out the animal model of disease, western blotting and drafted the manuscript. IF did the isolation of the extracellular vesicles and characterization by NTA; gut histology and performed bioinformatics analysis, together with MS, for graphical representation. ASC prepared GDE for MS analysis and RM was responsible for the mass spectrometry analysis and bioinformatics. Mass spectrometry was performed by HCB. MPM and BCS conceived the study, participated in its design and coordination and edited the manuscript. All authors read and approved the final manuscript.

Competing interests

The authors have declared no competing interests, except for MPM who serves on advisory board for Gilead Sciences.

Acknowledgements

This work was supported by the Fundação para a Ciência e Tecnologia (Grant No. PTDC/MEC-MET/29314/2017) awarded to MPM and BCS. IF is a recipient of Fundação para a Ciência e Tecnologia fellowship (PD/BD/114044/2015).

References

[1] IDF. IDF Diabetes Atlas Ninth. Dunia: IDF. 2019. 168 p.

[2] Rubino F, Nathan DM, Eckel RH, Schauer PR, Alberti KGMM, Zimmet PZ, et al. Metabolic surgery in the treatment algorithm for type 2 diabetes: A joint statement by international diabetes organizations. Diabetes Care. 2016;39(6):861–77.

[3] Aminian A, Vidal J, Salminen P, Still CD, Hanipah ZN, Sharma G, et al. Late relapse of diabetes after bariatric surgery: Not rare, but not a failure. Diabetes Care. 2020;43(3):534–40.

[4] Petersen MC, Shulman GI. Mechanisms of insulin action and insulin resistance. Physiol Rev. 2018;98(4):2133–223.

[5] Tabák AG, Herder C, Rathmann W, Brunner EJ, Kivimäki M. Prediabetes: A high-risk state for diabetes development. Lancet [Internet]. 2012;379(9833):2279–90

462 [6] Hamdy O, Tasabehji MW, Elseaidy T, Tomah S, Ashrafzadeh S, Mottalib A. Fat Versus
463 Carbohydrate-Based Energy-Restricted Diets for Weight Loss in Patients With Type 2 Diabetes.
464 Curr Diab Rep. 2018;18(12).

465 [7] Ban LA, Shackel NA, McLennan S V. Extracellular vesicles: A new frontier in biomarker
466 discovery for non-alcoholic fatty liver disease. Int J Mol Sci. 2016;17(3).

467 [8] Zhang J, Li S, Li L, Li M, Guo C, Yao J, et al. Exosome and exosomal microRNA:
468 Trafficking, sorting, and function. Genomics, Proteomics Bioinforma. 2015;13(1).

469 [9] Théry C, Zitvogel L, Amigorena S. Exosomes: composition, biogenesis and function. Nat
470 Rev Immunol. 2002;2(8):569–79.

471 [10] Deng Z, Poliakov A, Hardy RW, Clements R, Liu C, Liu Y, et al. Adipose Tissue
472 Exosome-Like Vesicles Mediate Activation of Macrophage-Induced Insulin Resistance.
473 2009;58 (November).

474 [11] Kranendonk MEG, Visseren FLJ, Van Herwaarden JA, Nolte-'t Hoen ENM, De Jager W,
475 Wauben MHM, et al. Effect of extracellular vesicles of human adipose tissue on insulin
476 signaling in liver and muscle cells. Obesity. 2014;22(10):2216–23.

477 [12] Chang X, Wang SL, Zhao SB, Shi YH, Pan P, Gu L, et al. Extracellular vesicles with
478 possible roles in gut intestinal tract homeostasis and IBD. Mediators Inflamm. 2020;2020.

479 [13] Smythies LE, Smythies JR. Exosomes in the gut. Front Immunol. 2014;5(MAR):2–5.

480 [14] Hu G, Gong AY, Roth AL, Huang BQ, Ward HD, Zhu G, et al. Release of Luminal
481 Exosomes Contributes to TLR4-Mediated Epithelial Antimicrobial Defense. PLoS Pathog.
482 2013;9(4).

483 [15] Chelakkot C, Choi Y, Kim DK, Park HT, Ghim J, Kwon Y, et al. Akkermansia
484 muciniphila-derived extracellular vesicles influence gut permeability through the regulation of
485 tight junctions. Exp Mol Med [Internet]. 2018;50(2):e450-11.

486 [16] Mallegol J, Van Niel G, Heyman M. Phenotypic and functional characterization of
487 intestinal epithelial exosomes. Blood Cells, Mol Dis. 2005;35(1):11–6.

488 [17] Evers SS, Sandoval DA, Seeley RJ. The Physiology and Molecular Underpinnings of the
489 Effects of Bariatric Surgery on Obesity and Diabetes. Annu Rev Physiol. 2017;79(1):313–34.

490 [18] Singh AK, Singh R, Kota SK. Bariatric surgery and diabetes remission: Who would have
491 thought it? Indian J Endocrinol Metab. 2015;19(5):563–76.

492 [19] David LA, Maurice CF, Carmody RN, Gootenberg DB, Button JE, Wolfe BE, et al. Diet
493 rapidly and reproducibly alters the human gut microbiome. Nature [Internet].
494 2014;505(7484):559–63.

495 [20] Burcelin R, Serino M, Chabo C, Blasco-Baque V, Amar J. Gut microbiota and diabetes:
496 From pathogenesis to therapeutic perspective. Acta Diabetol. 2011;48(4):257–73.

497 [21] Kowalski GM, Bruce CR. The regulation of glucose metabolism: Implications and
498 considerations for the assessment of glucose homeostasis in rodents. Am J Physiol - Endocrinol
499 Metab. 2014;307(10):E859–71.

500 [22] Kalra H, Drummen GPC, Mathivanan S. Focus on extracellular vesicles: Introducing the
501 next small big thing. Int J Mol Sci. 2016;17(2).

502 [23] Schwanhüusser B, Busse D, Li N, Dittmar G, Schuchhardt J, Wolf J, et al. Global
503 quantification of mammalian gene expression control. Nature. 2011;473(7347):337–42.

504 [24] Abumrad NA, Davidson NO. Role of the gut in lipid homeostasis. Physiol Rev.
505 2012;92(3):1061–85.

506 [25] Amir, Weber, Beard, Bomyea T. NIH Public Access. Bone [Internet]. 2008;23(1):1–7.

507 [26] Kipnis DM, Cori CF. Studies of Tissue Permeability. J Biol Chem [Internet].
508 1960;235(11):3070–5.

509 [27] Chernick SS, Chaikoff IL, Abraham S. Localization of initial block in glucose metabolism
510 in diabetic liver slices. J Biol Chem. 1951;193(2):793-802.
511
512 [28] Renold AE, Hastings AB, Nesbett FB. Studies on carbohydrate metabolism in rat liver
513 slices. III. Utilization of glucose and fructose by liver from normal and diabetic animals. J Biol
514 Chem. 1954;209(2):687-696.

515 [29] Da Silva D, Ausina P, Alencar EM, Coelho WS, Zancan P, Sola-Penna M. Metformin
516 reverses hexokinase and phosphofructokinase downregulation and intracellular distribution in
517 the heart of diabetic mice. IUBMB Life. 2012;64(9):766–74.

518 [30] Randle PJ, Garland PB, Hales CN, Newsholme EA. The Glucose Fatty-Acid Cycle Its
519 Role in Insulin Sensitivity and the Metabolic Disturbances of Diabetes Mellitus. Lancet.
520 1963;281(7285):785–9.

521 [31] Kelley DE, Mandarino LJ. Fuel selection in human skeletal muscle in insulin resistance: A
522 reexamination. Diabetes. 2000;49(5):677–83.

523 [32] Jangra S, Raja SK, Sharma RK, Pothuraju R, Mohanty AK. Ameliorative effect of
524 fermentable fibres on adiposity and insulin resistance in C57BL/6 mice fed a high-fat and
525 sucrose diet. Food Funct. 2019;10(6):3696–705.

526 [33] Hoffman S, Alvares D, Adeli K. Intestinal lipogenesis: How carbs turn on triglyceride
527 production in the gut. Curr Opin Clin Nutr Metab Care. 2019;22(4):284–8.

528 [34] Deng WJ, Nie S, Dai J, Wu JR, Zeng R. Proteome, phosphoproteome, and
529 hydroxyproteome of liver mitochondria in diabetic rats at early pathogenic stages. Mol Cell
530 Proteomics. 2010;9(1):100–16.

531 [35] Kanuri BN, Rebello SC, Pathak P, Agarwal H, Kanshana JS, Awasthi D, et al. Glucose and
532 lipid metabolism alterations in liver and adipose tissue pre-dispose p47phox knockout mice to
533 systemic insulin resistance. Free Radic Res [Internet]. 2018;52(5):568–82.

534 [36] Knebel B, Hartwig S, Haas J, Lehr S, Goeddeke S, Susanto F, et al. Peroxisomes
535 compensate hepatic lipid overflow in mice with fatty liver. Biochim Biophys Acta - Mol Cell
536 Biol Lipids [Internet]. 2015;1851(7):965–76.

537 [37] Wang F, Wu J, Qiu Z, Ge X, Liu X, Zhang C, et al. ACOT1 expression is associated with
538 poor prognosis in gastric adenocarcinoma. Hum Pathol [Internet]. 2018;77:35–44.

539 [38] Steensels S, Qiao J, Zhang Y, Maner-Smith KM, Kika N, Holman CD, et al. Acot9 traffics
540 mitochondrial short-chain fatty acids towards de novo lipogenesis and glucose production in the
541 liver. Hepatology. 2020;0–3.

542 [39] Alves-Bezerra M, Li Y, Acuña M, Ivanova AA, Corey KE, Ortlund EA, et al. Thioesterase
543 Superfamily Member 2 Promotes Hepatic VLDL Secretion by Channeling Fatty Acids Into
544 Triglyceride Biosynthesis. Hepatology. 2019;70(2):496–510.

545 [40] Ersoy BA, Maner-Smith KM, Li Y, Alpertunga I, Cohen DE. Thioesterase-mediated
546 control of cellular calcium homeostasis enables hepatic ER stress. J Clin Invest.
547 2018;128(1):141–56.

548 [41] Yamaguchi K, Yang L, McCall S, Huang J, Xing XY, Pandey SK, et al. Inhibiting
549 triglyceride synthesis improves hepatic steatosis but exacerbates liver damage and fibrosis in
550 obese mice with nonalcoholic steatohepatitis. Hepatology. 2007;45(6):1366–74.

551 [42] Fujita M, Momose A, Ohtomo T, Nishinosono A, Tanonaka K, Toyoda H, et al.
552 Upregulation of fatty acyl-CoA thioesterases in the heart and skeletal muscle of rats fed a high-
553 fat diet. Biol Pharm Bull. 2011;34(1):87–91.

554 [43] Franklin MP, Sathyanarayan A, Mashek DG. Acyl-CoA thioesterase 1 (ACOT1) regulates
555 PPARα to couple fatty acid flux with oxidative capacity during fasting. Diabetes.
556 2017;66(8):2112–23.

557 [44] Volpe CMO, Villar-Delfino PH, Dos Anjos PMF, Nogueira-Machado JA. Cellular death,
558 reactive oxygen species (ROS) and diabetic complications review-Article. Cell Death Dis.
559 2018;9(2).

560 [45] Luo W, Xu Q, Wang Q, Wu H, Hua J. Effect of modulation of PPAR-γ activity on Kupffer
561 cells M1/M2 polarization in the development of non-alcoholic fatty liver disease. Sci Rep.
562 2017;7(March):1–13.

563 [46] Yang CK, Wang XK, Liao XW, Han CY, Yu TD, Qin W, et al. Aldehyde dehydrogenase 1
564 (ALDH1) isoform expression and potential clinical implications in hepatocellular carcinoma.
565 PLoS One. 2017;12(8):1–13.

566 [47] Chen CH, Ferreira JCB, Gross ER, Mochly-Rosen D. Targeting aldehyde dehydrogenase 2:
567 New therapeutic opportunities. Physiol Rev. 2014;94(1):1–34.

568 [48] Van Goudoever JB, Stoll B, Henry JF, Burrin DG, Reeds PJ. Adaptive regulation of
569 intestinal lysine metabolism. Proc Natl Acad Sci U S A. 2000;97(21):11620–5.

570 [49] Azevedo C, Saiardi A. Why always lysine? The ongoing tale of one of the most modified
571 amino acids. Adv Biol Regul [Internet]. 2016;60:144–50.

572 [50] Khan L, Bamji MS. Tissue Carnitine Deficiency due to Dietary Lysine Deficiency:
573 Triglyceride Accumulation and Concomitant Impairment in Fatty Acid Oxidation. J Nutr.
574 1979;109(1):24–31.

575 [51] Liu H, Yu S, Xu W, Xu J. Enhancement of 26S proteasome functionality connects
576 oxidative stress and vascular endothelial inflammatory response in diabetes. Arterioscler Throm
577 Vasc Biol. 2012; 32(9):2131-2140.

578 [52] Rousseau A, Bertolotti A. Regulation of proteasome assembly and activity in health and
579 disease. Nat Rev Mol Cell Biol [Internet]. 2018;19(11):697–712.

580 [53] Cox J, Mann M. MaxQuant enables high peptide identification rates, individualized p.p.b.-
581 range mass accuracies and proteome-wide protein quantification. Nat Biotechnol.
582 2008;26(12):1367–72.

583 [54] Carvalho AS, Ribeiro H, Voabil P, Penque D, Jensen ON, Molina H, et al. Global mass
584 spectrometry and transcriptomics array based drug profiling provides novel insight into
585 glucosamine induced endoplasmic reticulum stress. Mol Cell Proteomics. 2014;13(12):3294–
586 307.

587

588

589

590

591

592

593

594

595

596

597

598

599

600

601

602

603

604

605

606 # Figure legends

607 **Figure 1 High fat diet induces prediabetes in mice and increases protein cargo in gut**
608 **derived EV**

609 **A**. Diet plan schematic representation. **B**. Body weight (n=20 per group). **C**. Representative Hematoxylin-
610 Eosin images of liver histological sections of NCD and HD mice. White areas indicated by black arrows
611 are lipid droplets, revealing steatosis in the liver of mice subjected to HD. **D.** Plasma glucose profile (md/dl)
612 along a glucose tolerance test (GTT) at different time points after glucose bolus (0, 15, 30, 60, 90, 120
613 minutes) at week 17 of age. **E**. Mean area under the curve of the GTT. Results are expressed as mean ±
614 SEM; n=20 per group. Unpaired t test with Welch's correction for B and D; ****p<0.0001. **F**. Gut cross
615 sections, EVs are labelled in green (CD81) and nuclei in blue (DAPI). NCD gut tissue in the left and HD
616 gut tissue in the right. CD81 quantification in the gut. **G**. Immunoblotting of gut tissue and gut derived EV
617 (GDE) isolated from NCD and HD mice. Protein extracts prepared from gut (10 μg) and from GDE (15
618 μg) were analyzed by western blotting using antibodies against EV marker CD63 and β-actin. **H**. Size and
619 concentration distribution of GDE determined by nanoparticle tracking analysis (NTA). A representative
620 NTA graph of GDE of mice fed with NCD (NCD-EV) (left) and HD (HD-EV) (right). **I**. Analysis of the
621 number of particles per mL of sample. **J.** Protein quantification in GDE in mg per mL of sample, obtained
622 by BCA. **K.** Protein content per GDE, represented in mg of protein per particle. Results are expressed as
623 mean ± SEM; n=17 for NCD-EV and n=25 for HD-EV. Unpaired t test with Welch's correction (F, I, J,
624 K); ***p<0.0005, **p<0.005.
625

626 **Figure 2 Study flow of proteomic approach for characterization of gut derived EV**
627 **protein cargos**

628 **A**. Strategy used for selection of proteins to be analyzed with confidence. **B**. Volcano plot representing the
629 fold change and adj.p-value in the gut-derived EV (GDE) isolated from prediabetic mice and control
630 groups. x-axis represents fold change, and y-axis adj.p-value. Dotted line sets the threshold of adj.p-
631 value<0.05. In grey are the non-regulated proteins, in black the 558 regulated proteins.
632

633 **Figure 3 Characterization of prediabetic gut derived EV by GO and KEGG**
634 **enrichment analysis directly against mouse annotation, according to GO terms**

635 **A**. Molecular function analysis of the GDE identified proteins. GO enrichment analysis according to
636 Molecular Function. **B**. Analysis of the main biological regulated by the proteins identified in the GDE.
637 GO enrichment analysis according to Biological Process. **C**. KEGG enrichment analysis for KEGG
638 pathway. **D**. GO enrichment analysis according to Cellular Compartment. On the left panels, changes are
639 displayed as the number of proteins with increased (red) or decreased (blue) levels (horizontal axis). On
640 the right panels, the horizontal axis indicates the significance -log10 (p-value) of the functional association,
641 which is dependent on the number of submitted proteins in the class, the number of proteins annotated in
642 the class, the total number of submitted proteins and the total number of mouse proteins.

643

644 **Figure 4 Cluster analysis of the top50 altered proteins of gut derived EV in**
645 **prediabetic mice**

646 **A**. Volcano plot representing the fold change and adj.p-value of gut-derived EV (GDE) proteins isolated
647 from prediabetic mice and control groups. x-axis represents fold change, and y-axis adj.p-value. Dotted line
648 sets the threshold of adj.p-value<0.0001, highlighting the most altered proteins in GDE from HD comparing
649 with GDE from NCD. In blue are the most down regulated proteins and in red the most upregulated. **B**.
650 Heatmap representing mean-centered abundance of the most altered proteins decorated in the previous
651 volcano plot. **C**. Violin plot demonstrating the fold changes of the most altered proteins and correspondent
652 cellular functions. Cellular metabolic process (GO) represented in green.

653

654 **Figure 5 Overview of prediabetes impact on gut derived EV proteome**

655 The identified proteins with higher differential expression are represented in the image according to their
656 function and estimated subcellular localization. Red color for proteins upregulated and blue color for
657 proteins down regulated in small intestine derived EV of mice fed with HD compared with controls, mice
658 fed with NCD. ROS, reactive oxygen species; TCA, tricarboxylic acid cycle. Image done in BioRender.

659 # Tables

660 **Table 1 Biological function of the main up and down regulated proteins in HD-GDE**
661 **compared with NCD-GDE by proteomics**

662

663 **Supplementary material**

664 **Supplementary Figure 1 Study flow of proteomic approach for characterization of gut**
665 **derived EV protein cargos**

666 **A**. Schematic representation of the detailed protocol used for isolation of GDE. Image done in
667 BioRender.

668 **B.** Schematic representation of the experimental process of analysis of gut derived EV (GDE).
669 Image done in BioRender. **C**. Bar plot indicating the number of proteins uniquely identified from
670 different species when searched against all proteins from all species in UniProt. **D**. Picture of LB-
671 agar (without antibiotics) petri dish after 24 after hours of inoculation with media where guts were
672 deposit overnight at 37ºC prior to EVs isolation.

673

674 **Supplementary Figure 2 Protein-protein interaction network**

675 The network was built using the STRING online software with a medium confidence level (0.4).
676 Each circle represents one protein. The line thickness indicates the strength of the evidence, with
677 thicker connections indicating higher confidence in the protein-protein interaction. Green circles
678 represent the proteins belonging to cellular metabolic process according to GO enrichment
679 analysis for biological processes.
680
681 **Supplementary Figure 3 Individual protein alteration levels according to its biological**
682 **function**
683 Data plots demonstrating the log fold changes of each protein in the image in accordance to its
684 related pathway.
685
686 **Supplementary File 1 List of proteins identified in gut derived EV proteomics**
687 Pdf format document. Description by columns: Pro- protein headers; Sample names – 18 columns
688 with quantitative values named with sample names (9 columns of NCD samples replicas, 9
689 columns of HD sample replicas); mean_C – mean expression for controls (NCD-GDE); mean_T
690 – mean expression for treated (HD-GDE); GN – gene name; logFC – log2fold change; AveExp
691 – average expression; t – t value; P.value – Pvalue; adj.P.value – adjusted P value using BH; B –
692 B-value. In red is highlighted the upregulated proteins; in blue the down regulated proteins and
693 in purple the missing values; when two colors are present is because one protein was identified
694 as up or down regulated, but it had an acquisition of zero, therefore is was excluded.
695

Figure 1

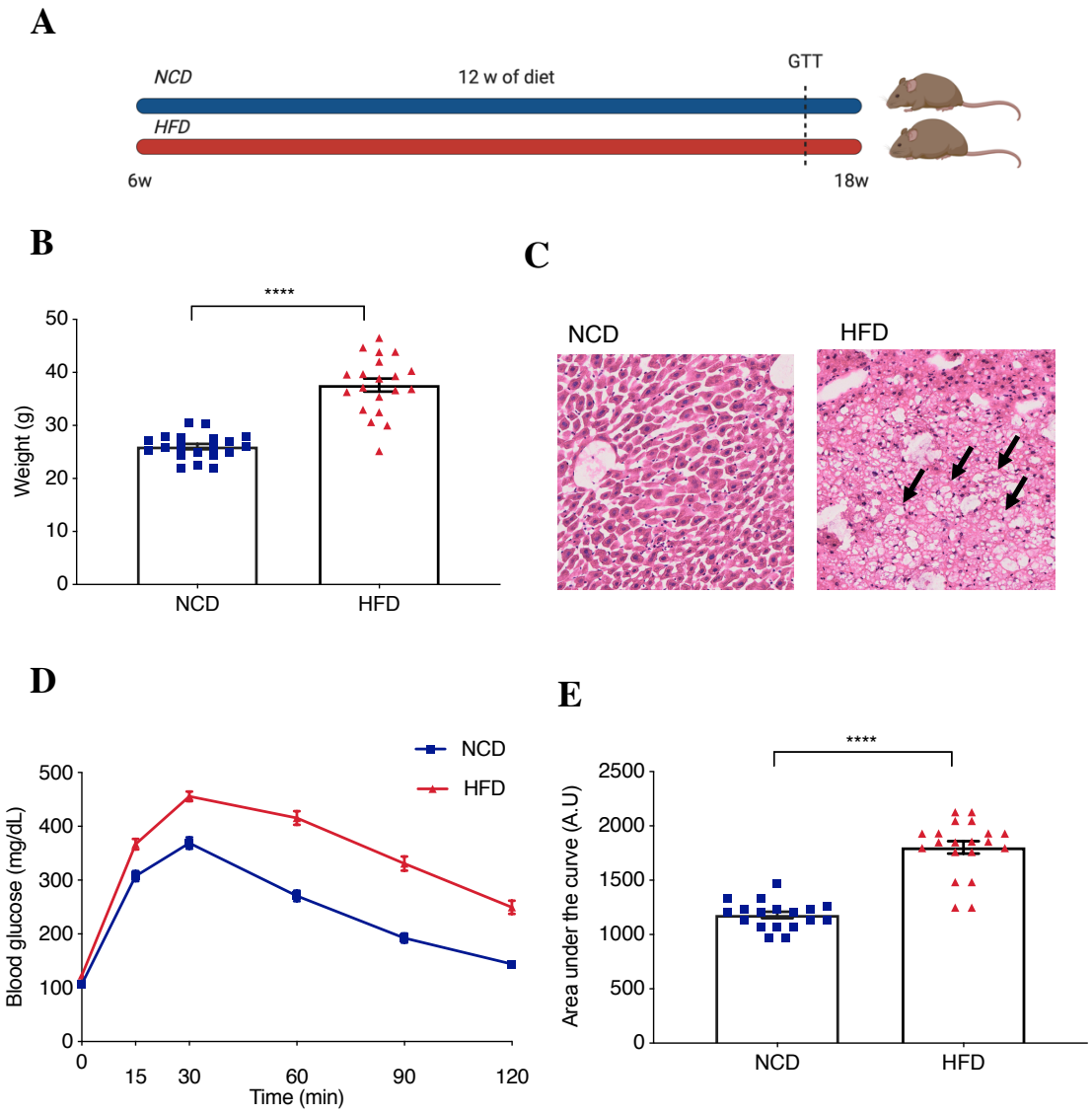
A
NCD
12 w of diet
GTT
HFD
6w
18w
B
****
Weight (g)
50
40
30
20
10
0
NCD
HFD
C
NCD
HFD
D
NCD
HFD
Blood glucose (mg/dL)
500
400
300
200
100
0
0
15
30
60
90
120
Time (min)
E
****
Area under the curve (A.U)
2500
2000
1500
1000
500
0
NCD
HFD

Figure 2

A

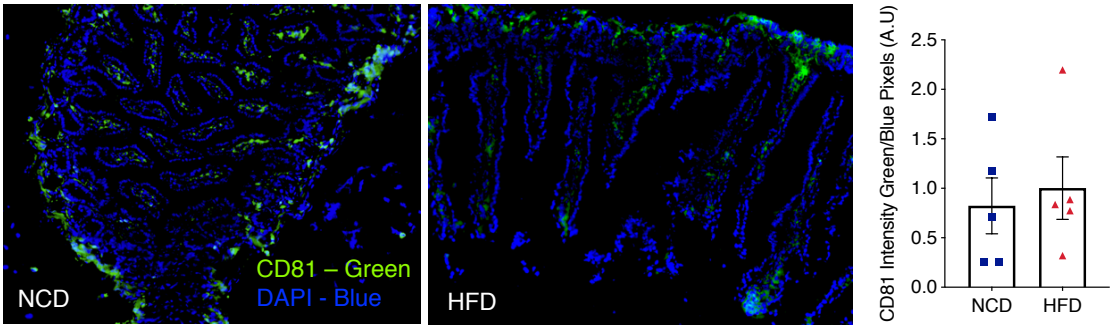

B

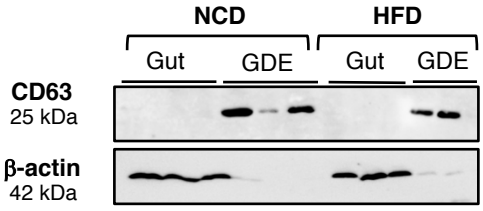

C

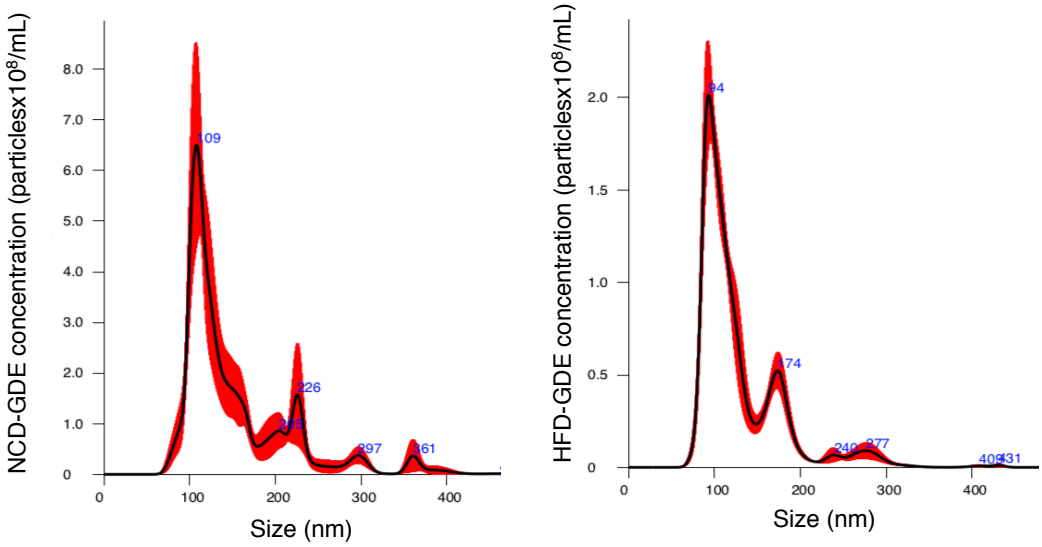

D

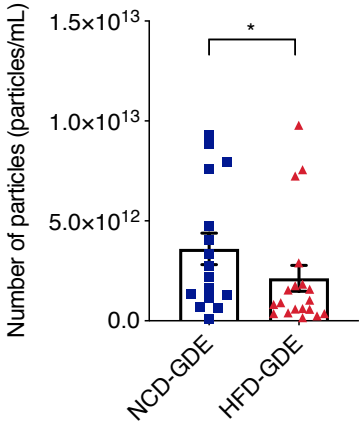

E

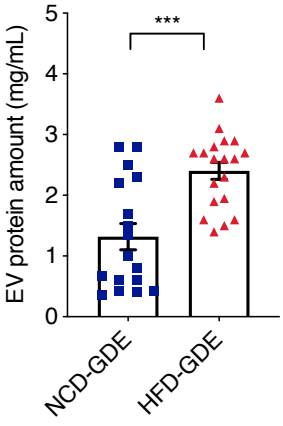

F

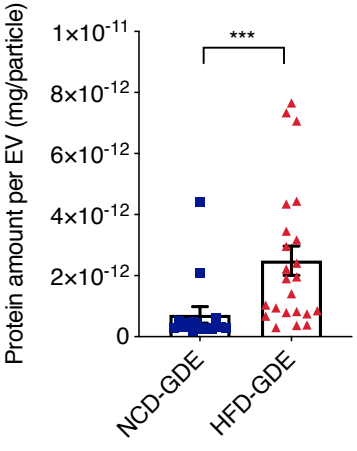

Figure 3

A

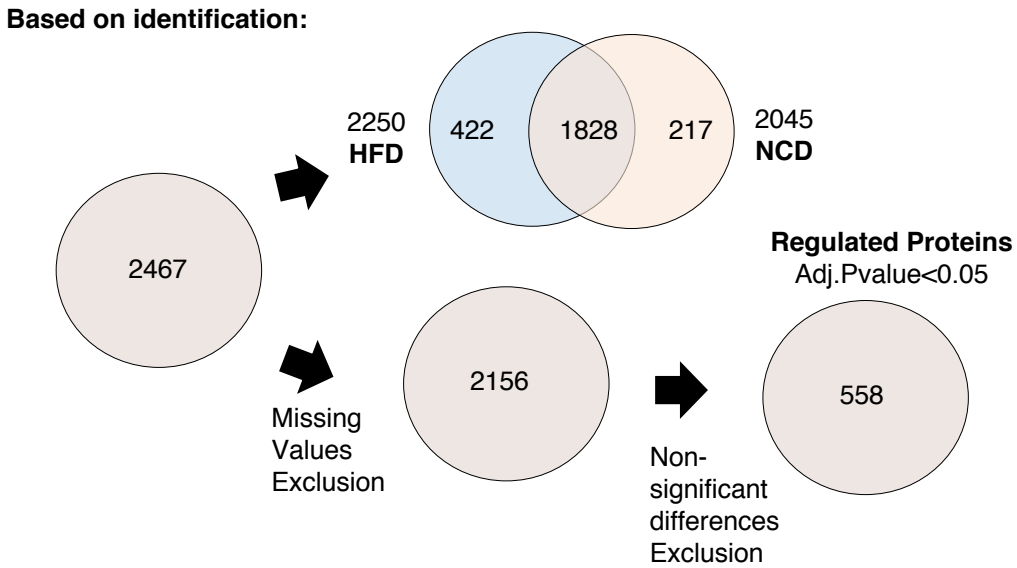
Based on identification:
2467
2250
HFD
422
1828
217
2045
NCD
Missing
Values
Exclusion
2156
Non-
significant
differences
Exclusion
Regulated Proteins
Adj.Pvalue<0.05
558

B

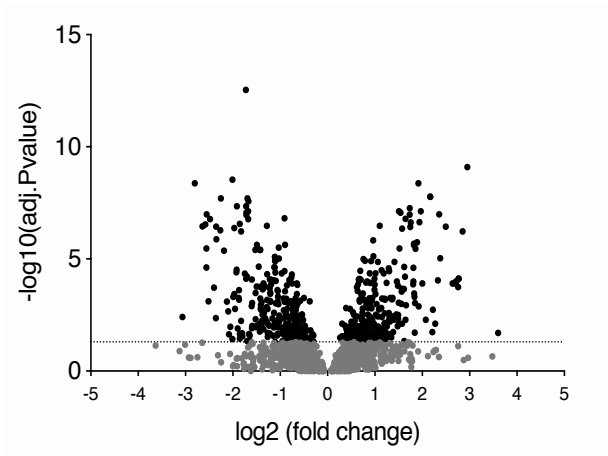
-log10(adj.Pvalue)
15
10
5
0
-5
-4
-3
-2
-1
0
1
2
3
4
5
log2 (fold change)

Figure 4

A

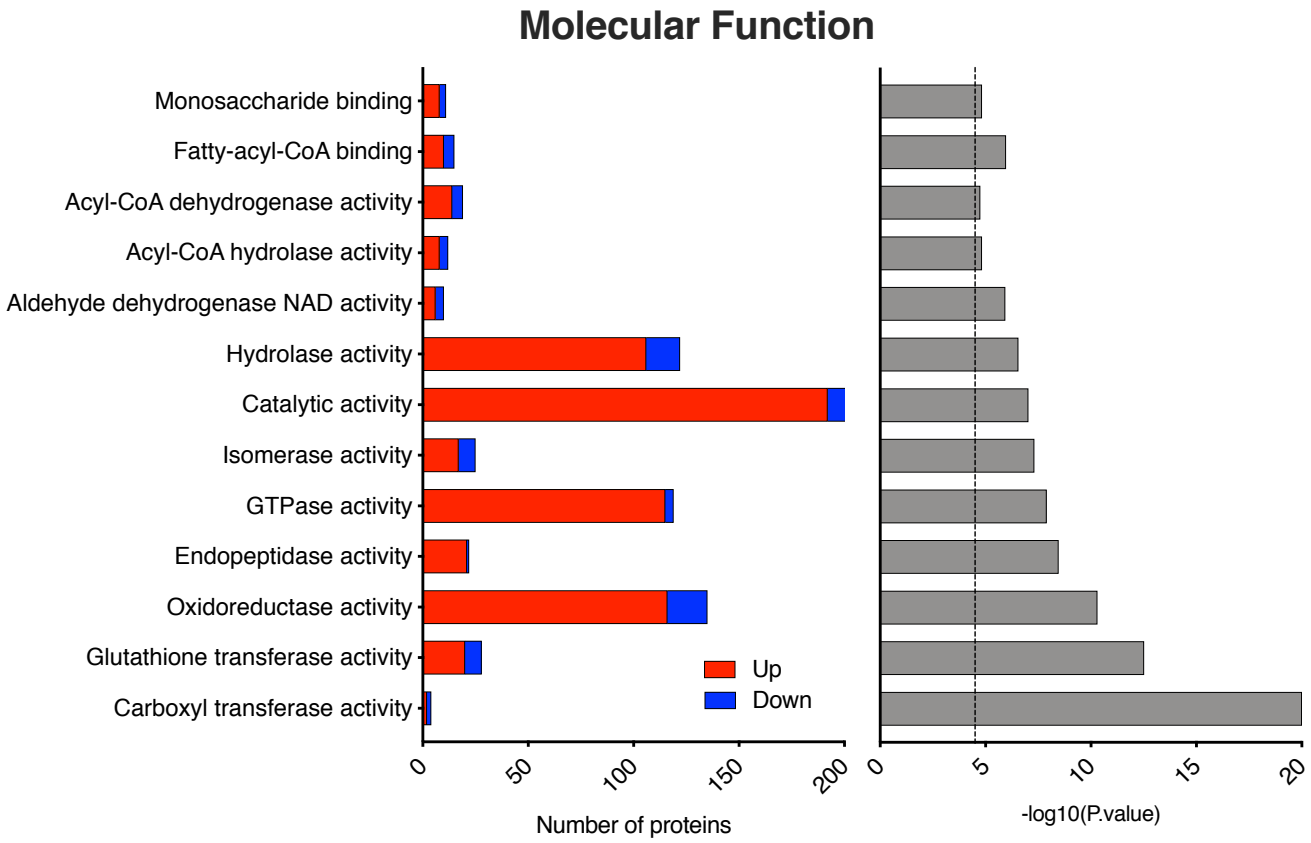
Molecular Function
Monosaccharide binding
Fatty-acyl-CoA binding
Acyl-CoA dehydrogenase activity
Acyl-CoA hydrolase activity
Aldehyde dehydrogenase NAD activity
Hydrolase activity
Catalytic activity
Isomerase activity
GTPase activity
Endopeptidase activity
Oxidoreductase activity
Glutathione transferase activity
Carboxyl transferase activity
Up
Down
0
50
100
150
200
Number of proteins
0
5
10
15
20
-log10(P.value)

B

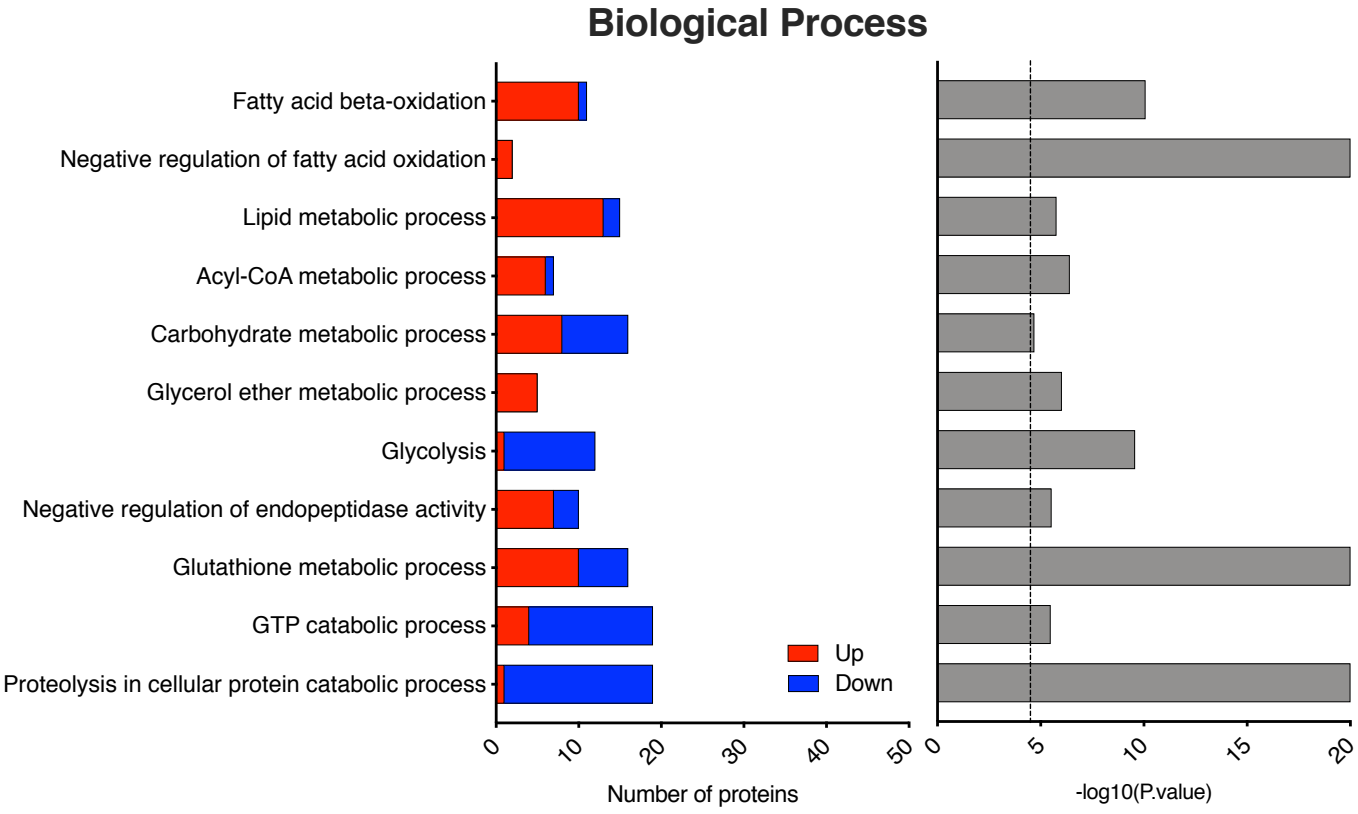
Biological Process
Fatty acid beta-oxidation
Negative regulation of fatty acid oxidation
Lipid metabolic process
Acyl-CoA metabolic process
Carbohydrate metabolic process
Glycerol ether metabolic process
Glycolysis
Negative regulation of endopeptidase activity
Glutathione metabolic process
GTP catabolic process
Proteolysis in cellular protein catabolic process
Up
Down
0
10
20
30
40
50
Number of proteins
0
5
10
15
20
-log10(P.value)

C

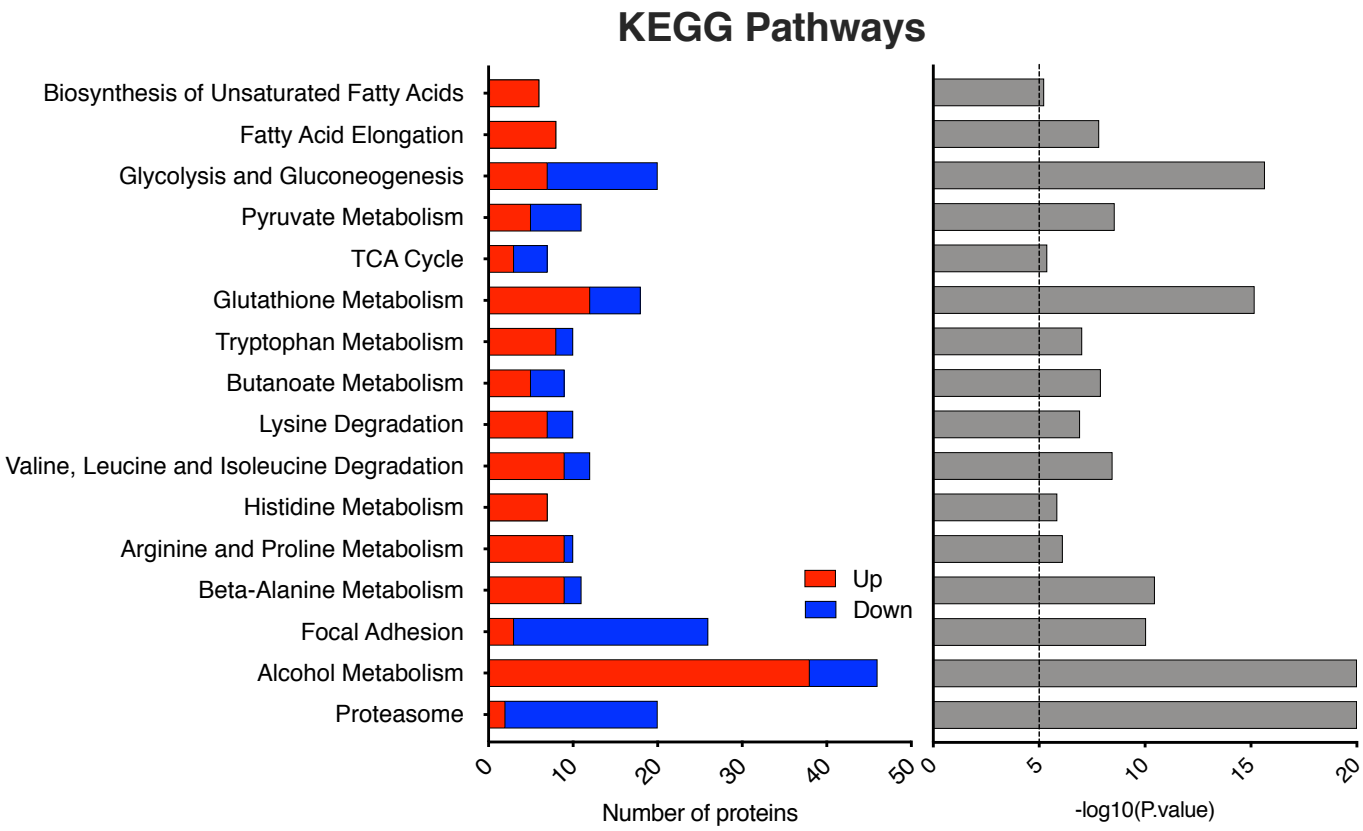
KEGG Pathways
Biosynthesis of Unsaturated Fatty Acids
Fatty Acid Elongation
Glycolysis and Gluconeogenesis
Pyruvate Metabolism
TCA Cycle
Glutathione Metabolism
Tryptophan Metabolism
Butanoate Metabolism
Lysine Degradation
Valine, Leucine and Isoleucine Degradation
Histidine Metabolism
Arginine and Proline Metabolism
Beta-Alanine Metabolism
Focal Adhesion
Alcohol Metabolism
Proteasome
Up
Down
0
10
20
30
40
50
Number of proteins
0
5
10
15
20
-log10(P.value)

D

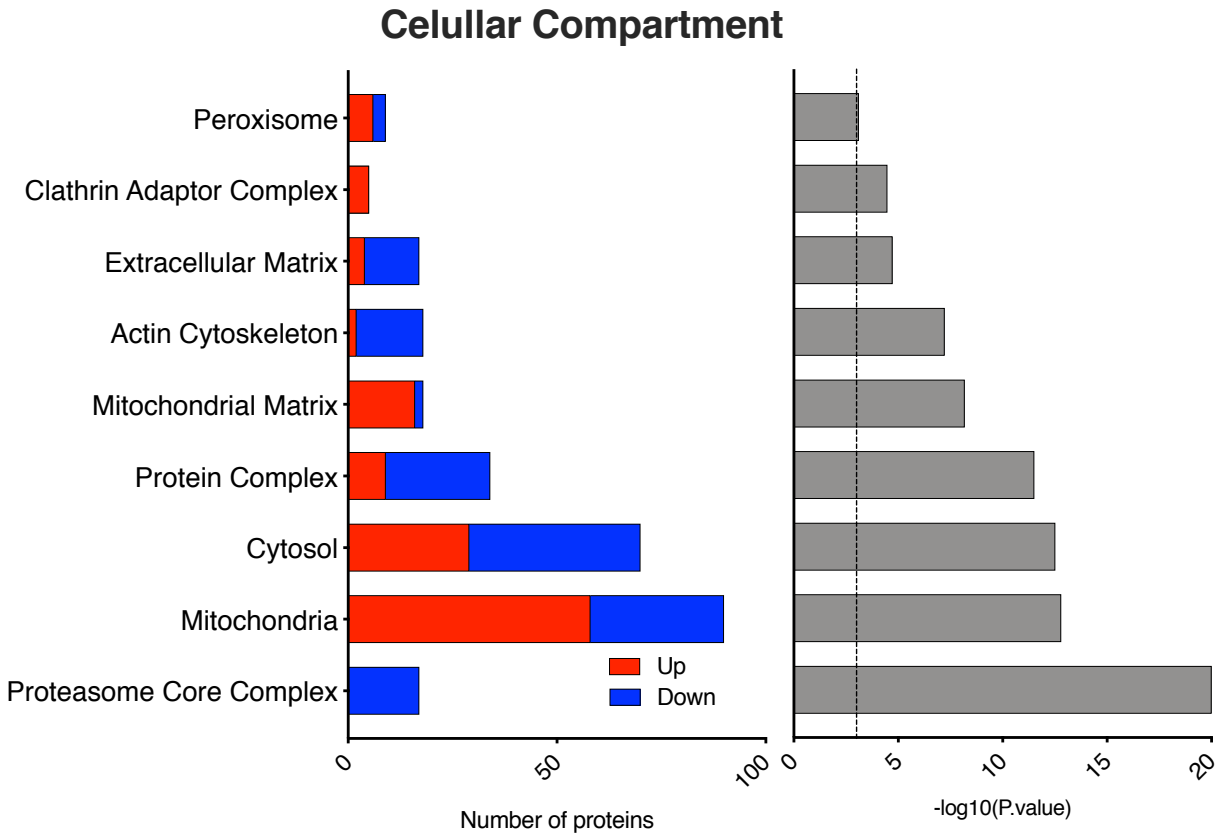
Celullar Compartment
Peroxisome
Clathrin Adaptor Complex
Extracellular Matrix
Actin Cytoskeleton
Mitochondrial Matrix
Protein Complex
Cytosol
Mitochondria
Proteasome Core Complex
Up
Down
0
50
100
Number of proteins
0
5
10
15
20
-log10(P.value)

Figure 5

A

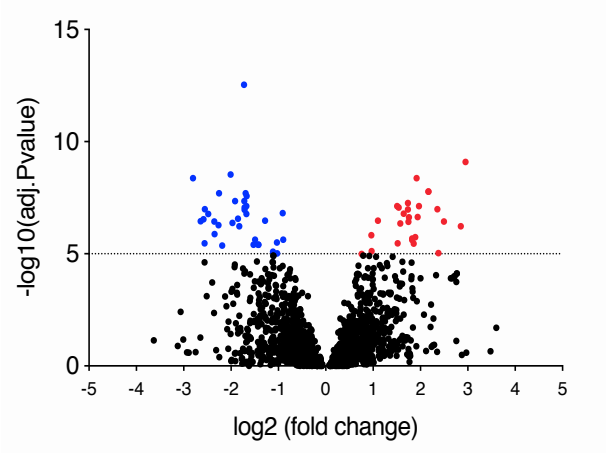
-log10(adj.Pvalue)
log2 (fold change)

C

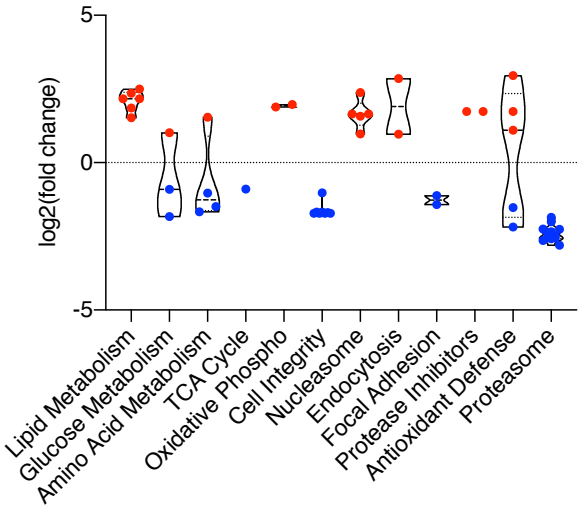
log2(fold change)
Lipid Metabolism
Glucose Metabolism
Amino Acid Metabolism
TCA Cycle
Oxidative Phospho
Cell Integrity
Nucleasome
Endocytosis
Focal Adhesion
Protease Inhibitors
Antioxidant Defense
Proteasome

B

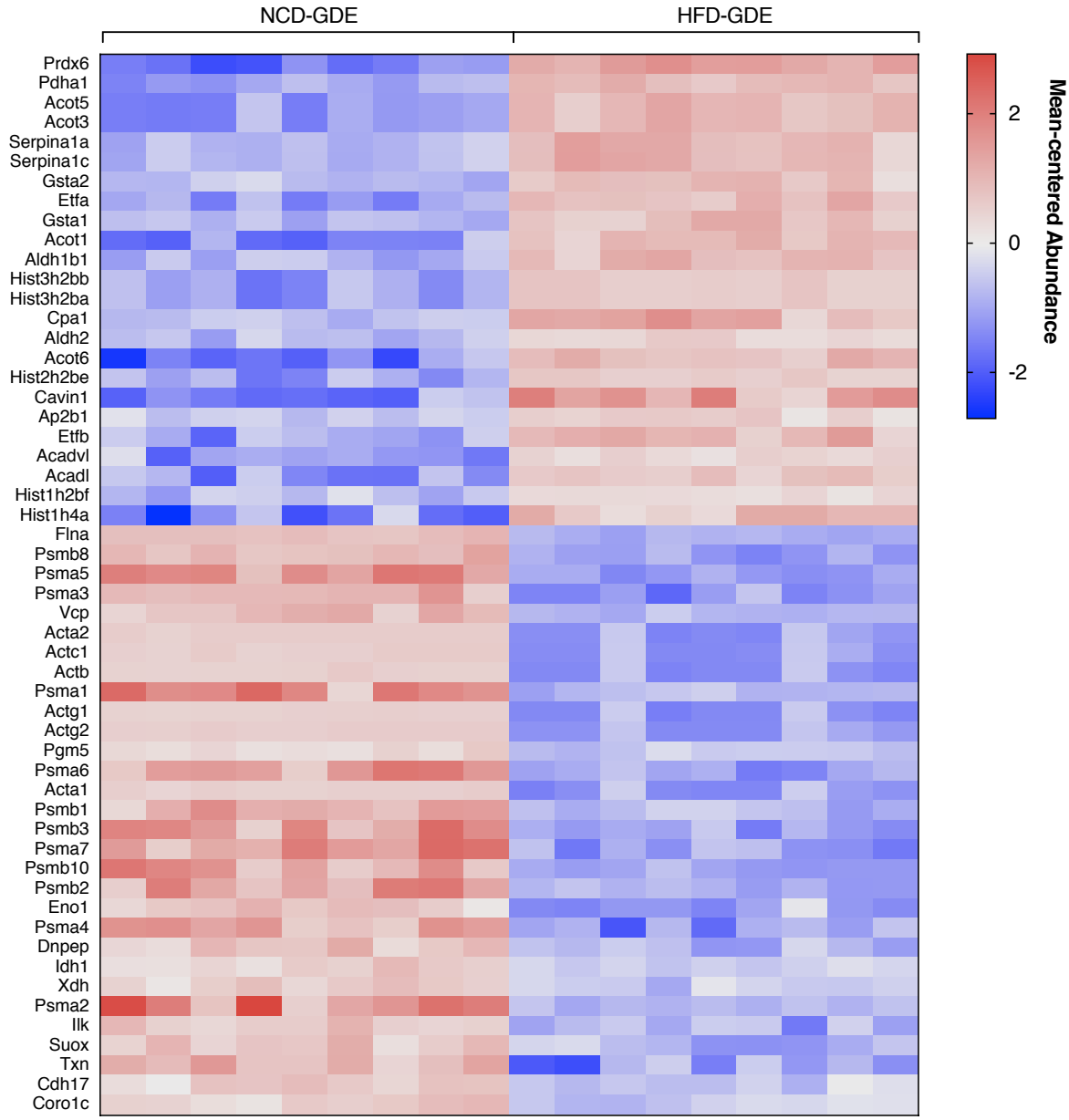
NCD-GDE
HFD-GDE
Prdx6
Pdha1
Acot5
Acot3
Serpina1a
Serpina1c
Gsta2
Etfa
Gsta1
Acot1
Aldh1b1
Hist3h2bb
Hist3h2ba
Cpa1
Aldh2
Acot6
Hist2h2be
Cavin1
Ap2b1
Etfb
Acadvl
Acadl
Hist1h2bf
Hist1h4a
Flna
Psmb8
Psma5
Psma3
Vcp
Acta2
Actc1
Actb
Psma1
Actg1
Actg2
Pgm5
Psma6
Acta1
Psmb1
Psmb3
Psma7
Psmb10
Psmb2
Eno1
Psma4
Dnpep
Idh1
Xdh
Psma2
Ilk
Suox
Txn
Cdh17
Coro1c
Mean-centered Abundance

Figure 6

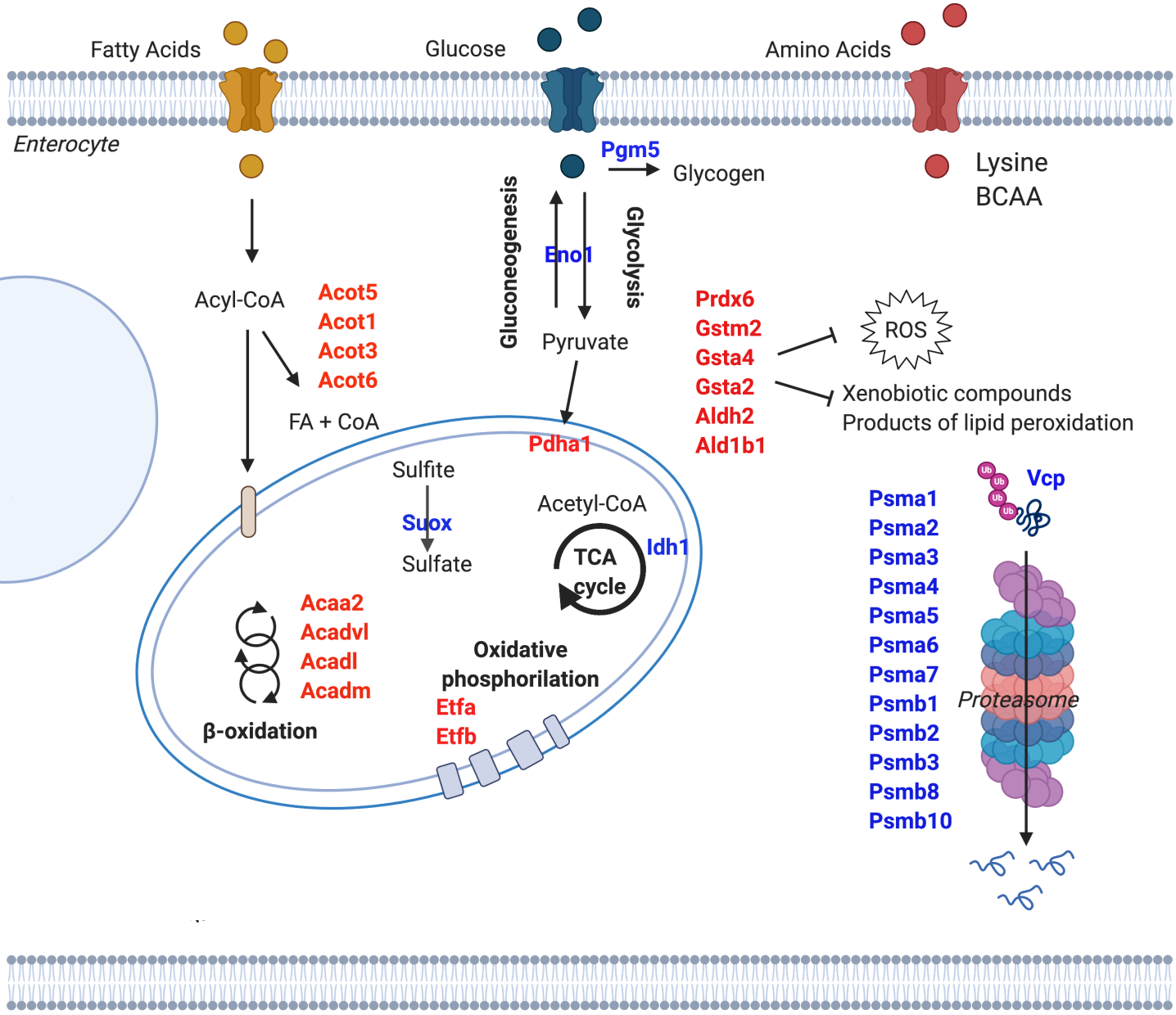
Fatty Acids
Glucose
Amino Acids
Enterocyte
Pgm5
Glycogen
Lysine
BCAA
Gluconeogenesis
Eno1
Glycolysis
Acyl-CoA
Acot5
Acot1
Acot3
Acot6
Pyruvate
Prdx6
Gstm2
Gsta4
Gsta2
Aldh2
Ald1b1
ROS
Xenobiotic compounds
Products of lipid peroxidation
FA + CoA
Pdha1
Sulfite
Suox
Sulfate
Acetyl-CoA
TCA cycle
Idh1
Vcp
Psma1
Psma2
Psma3
Psma4
Psma5
Psma6
Psma7
Psmb1
Psmb2
Psmb3
Psmb8
Psmb10
Proteasome
Acaa2
Acadvl
Acadl
Acadm
β-oxidation
Oxidative phosphorilation
Etfa
Etfb

Suplemmentary Fig. 1

A

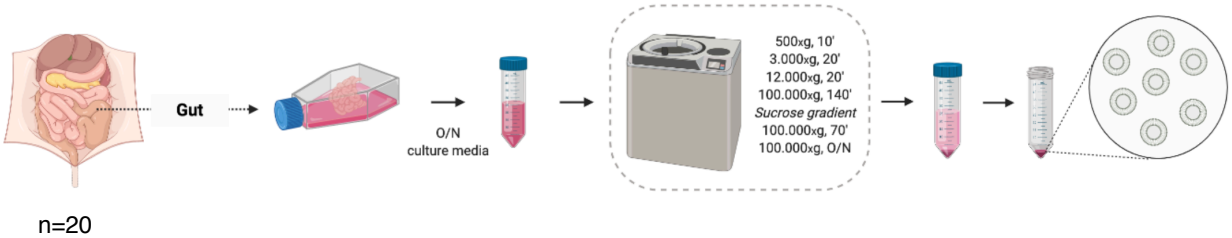

n=20

B

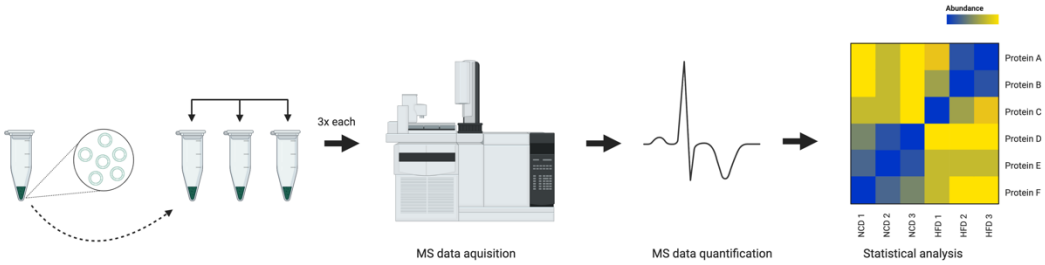

C

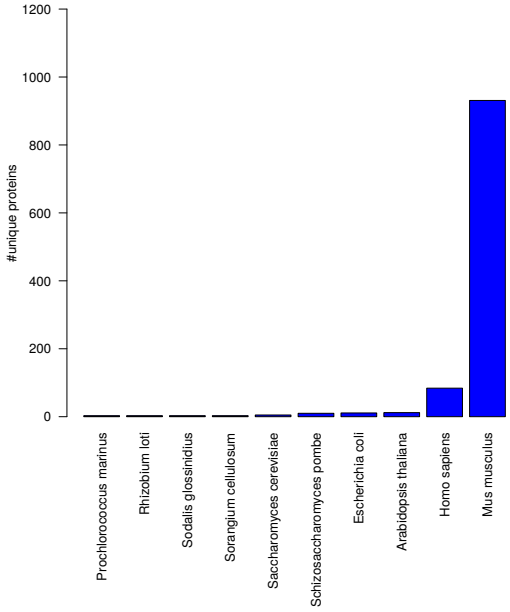

D

Suplemmentary Fig. 2

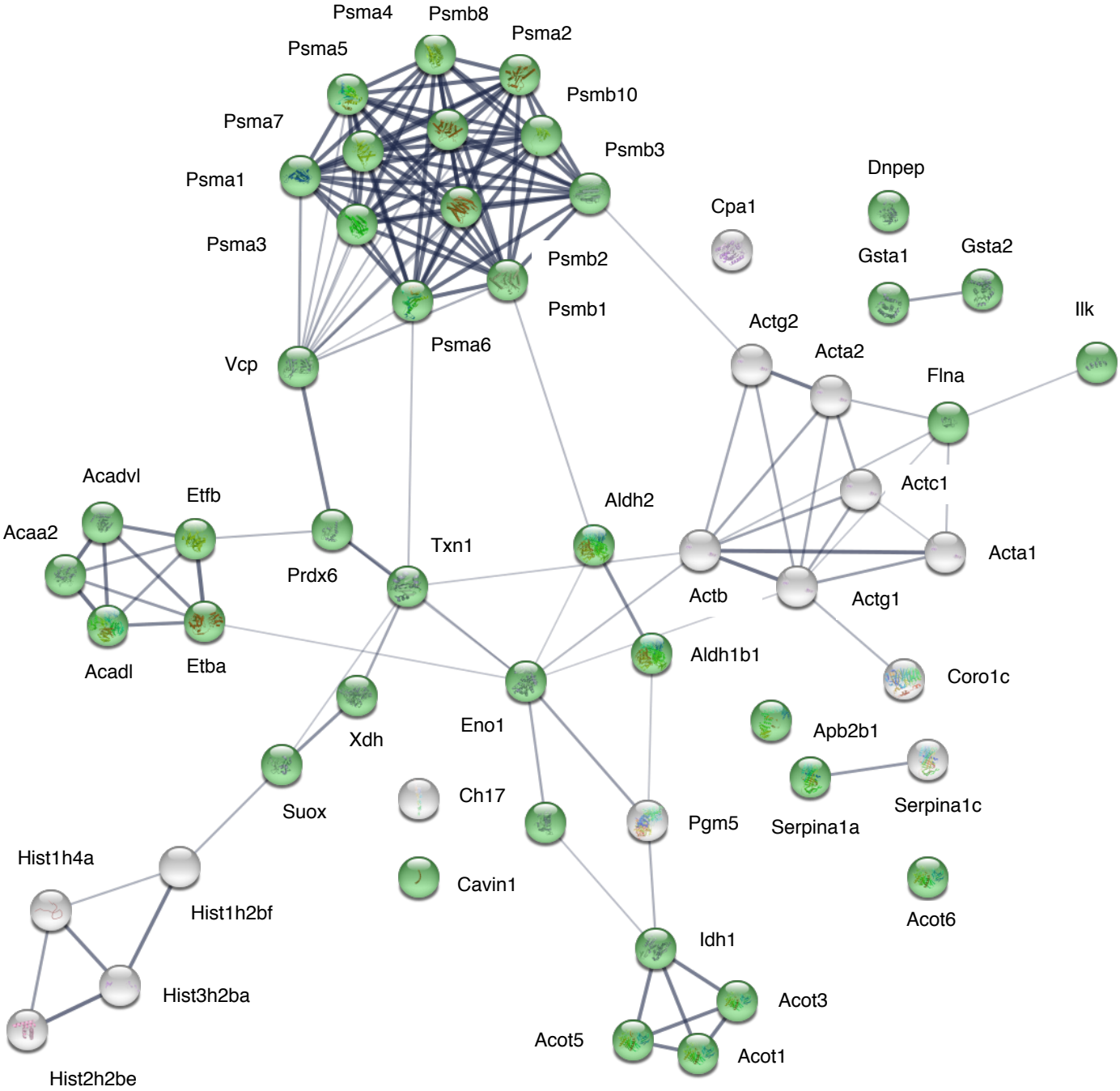

Suplemmentary Fig. 3

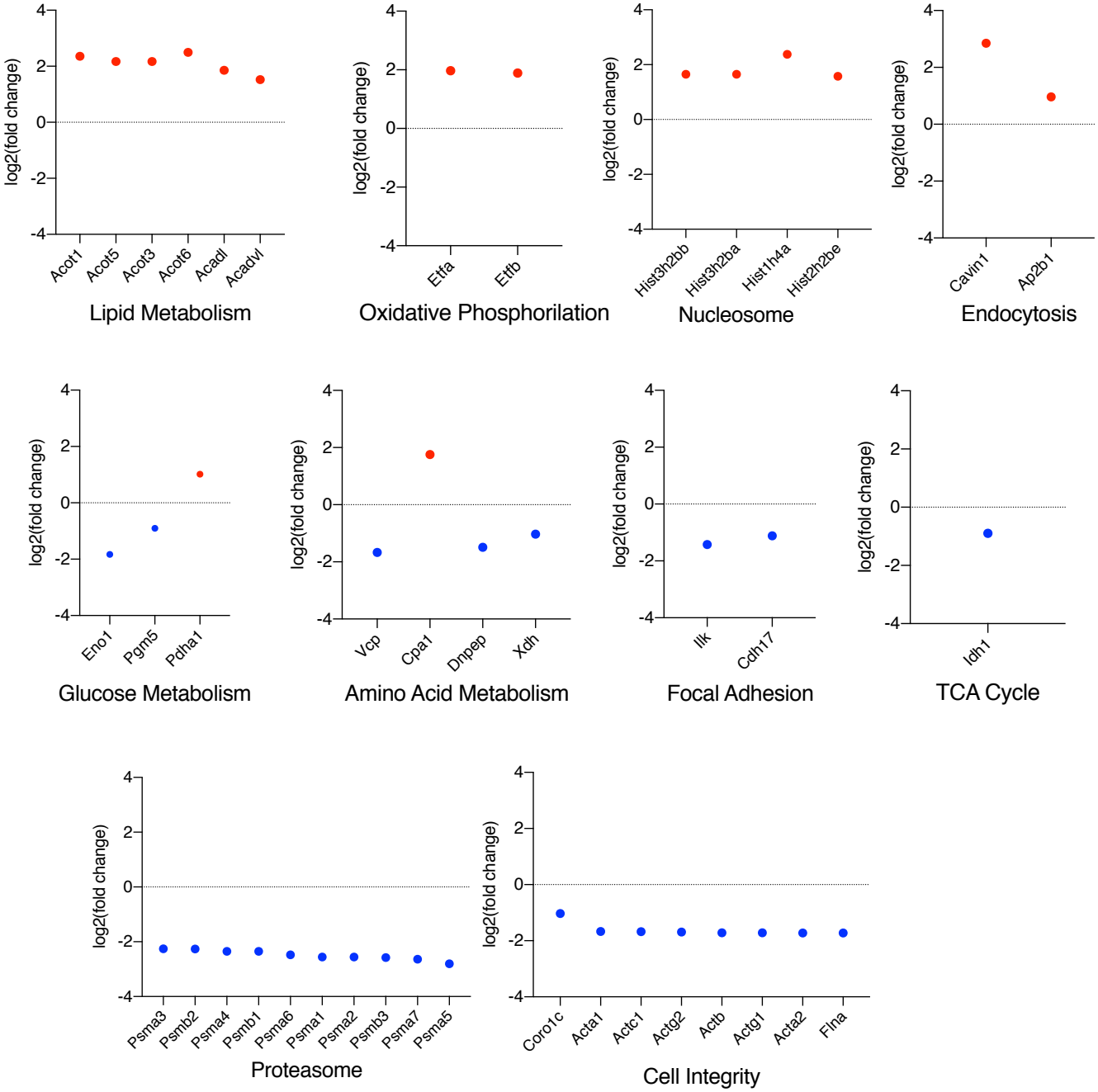

Table 1

Biological Function	Up	Down
Lipid Metabolism		
Mitochondrial ß-oxidation	ACADVL; ACADL	
Lipid Homeostasis	ACOT1; ACOT2; ACOT3; ACOT5; ACOT6	
Glucose Metabolism		
Glycolysis		ENO1; PGM5
Conversion of pyruvate to acetyl-CoA	PDHA1	
Amino Acid Metabolism		
C-terminal amino acid release	CPA1	
Protein degradation		VCP
Peptide metabolism		DNPEP
Purine Metabolism		XDH
TCA Cycle		IDH1
Oxidative phosphorylation	ETFA; ETFB	
Cell Integrity		ACTA1; ACTA2; ACTB; ACTC1; ACTG1; ACTG2; CORO1C; FLNA
Nucleosome	HIST1H4A; HIST3H2BB; HIST3H2BA; HIST2H2BE; HIST1H2BF	
Endocytosis		
Caveolar endocytosis	CAVIN1	
Clathrin-dependent endocytosis	AP2B1	
Focal adhesion		ILK; CDH17
Protease inhibitor	SERPINA1A; SERPINA1C	
Antioxidant Defense	PRDX6; GSTA4; GSTA1; GSTA2; ALDH2; ALDH1B1	TXN; SUOX
Proteasome		PSMA1; PSMA2; PSMA3; PSMA4; PSMA5; PSMA6; PSMA7; PSMB1; PSMB2; PSMB3; PSMB8; PSMB10